Journal of The Electrochemical Society, **146** (5) 1696-1701 (1999)
S0013-4651(98)08-024-0 CCC: $7.00 © The Electrochemical Society, Inc.

Structure and Lithium Insertion Properties of Carbon Nanotubes

G. T. Wu,[a] C. S. Wang,[b,*] X. B. Zhang,[b] H. S. Yang,[a] Z. F. Qi,[a] P. M. He,[a] and W. Z. Li[a]

[a]*Department of Physics and* [b]*Department of Materials Science and Engineering, Zhejiang University, Hangzhou 310027, China*

Carbon nanotubes were obtained by pyrolysis of acetylene or ethylene catalyzed by iron or iron oxide nanoparticles. The morphology, microstructure, and lithium insertion properties of these carbon nanotubes were investigated by transmission electron microscopy, high-resolution transmission electron microscopy, X-ray diffraction, Raman spectroscopy, and electrochemical measurements, respectively. The results showed that the structures of the carbon nanotubes play major roles in both specific capacity and cycle life. Slightly graphitized carbon nanotubes showed a specific capacity of 640 mAh/g during the first charge, whereas well-graphitized carbon nanotubes showed a specific capacity of 282 mAh/g during the first charge. After 20 charge/discharge cycles the charge capacity of the slightly graphitized samples degraded to 65.3% of their original charge capacities, but the well-graphitized samples maintained 91.5% of their original charge capacities. The effects of charge-discharge rates and cycling temperature on lithium insertion properties of carbon nanotubes with different extents of graphitization are discussed.
© 1999 The Electrochemical Society. S0013-4651(98)08-024-0. All rights reserved.

Manuscript submitted August 10, 1998; revised manuscript received November 12, 1998.

Carbon nanotubes, a new form of elemental carbon, were discovered by Iijima[1] in 1991 in cathode-tip deposits during the arc-discharge synthesis of fullerenes. Later, large quantities of carbon nanotubes were produced by the arc-discharge method[2] or pyrolyzing hydrocarbons.[3,4] According to the accepted "Russian doll" model, carbon nanotubes are composed of graphitic sheets rolled into closed concentric cylinders with diameters on the order of nanometers and lengths on the order of micrometers.[1] Electron[1,5] and X-ray diffraction studies[5] of carbon nanotubes showed that the distances between the graphitic sheets are larger by a few percent than those in bulk graphite. However, the Russian doll model is oversimplified. Defects of various types were apparent in published HRTEM images of carbon nanotubes.[1-4] Detailed X-ray powder diffraction measurements[6] on carbon nanotubes demonstrated the existence of short-range interlayer stacking correlations and suggested that there were correlated flat graphitic regions in the carbon nanotubes, which should not be observable in idealized models of carbon nanotubes. Bulk physical and chemical property measurements also showed that carbon nanotubes were highly defective and had a local structure similar to turbostratic graphite.[7]

Raman spectroscopy is a powerful and sensitive technique for studying the structures of carbonaceous materials. For single-crystal graphite, a strong Raman line at 1580 cm^{-1} is observed.[8] The hexagonal graphite crystal belongs to the space group D_{6h}^4, and the irreducible representations of the vibrational modes are expressed as $\Gamma = 2E_{2g} + E_u + A_{2u} + B_{2g}$. Among them only two E_{2g} modes are Raman active. The Raman line at 1580 cm^{-1} corresponds to one of the E_{2g} modes,[8] which is often designated as the G line. Polycrystalline graphite and disordered carbon exhibit an additional line at 1350 cm^{-1} designated as the D line.[8] The 1350 cm^{-1} mode is Raman allowed due to the relaxation of the wave-vector selection rule resulting from finite crystal size effects.[8] Several Raman studies of carbon nanotubes have been used[9-11] to investigate the structure of carbon nanotubes. The Raman spectra of multiwall carbon nanotubes[9,10] exhibited only two lines at about 1350 and 1580 cm^{-1} corresponding to the D and G line of polycrystalline graphite. However, slight but significant differences in the relative intensities, energies, and widths as well in resonance behavior were found for the Raman lines of carbon nanotubes and polycrystalline graphite.[9]

Most carbonaceous materials can react reversibly with Li to some extent, therefore they can be used as negative electrodes in lithium-ion batteries.[12] Carbon nanotubes produced by the arc-discharge method have been evaluated for this application.[13] Nalimova et al.[14] also studied Li interaction with pyrolytic carbon nanotubes under high-pressure conditions. However the electrochemical performance of lithium insertion into pyrolytic carbon nanotubes has been little investigated as yet. In this work, we report data for the electrochemical Li insertion into pyrolytic carbon nanotubes. The performance of pyrolytic carbon nanotubes is shown to be critically dependent on the structure of pyrolytic carbon nanotubes.

Experimental

Catalytic synthesis of carbon nanotube.—The carbon nanotubes used in this work were synthesized by the catalytic decomposition of acetylene or ethylene at 700°C over iron nanoparticles or iron oxide nanoparticles. Catalytic particles with sizes of tens of nanometers were made by deoxidizing mechanical-milled iron oxide to iron or by a sol-gel process using $FeCl_3$ as the starting material to produce iron oxide. Reactions were carried out in a fixed-bed flow reactor, which was composed of a ceramic boat containing 20 mg of catalyst placed in a horizontal quartz tube. A mixture of 5% acetylene or ethylene in H_2 was introduced into the quartz tube at a rate of 200 mL/min for 40 min during the reactions. The as-formed carbon nanotubes were held in dilute HNO_3 for 4 h to dissolve the catalyst. Then they were filtered, washed with distilled water, and dried at 150°C under vacuum. C (carbon), H (hydrogen), and N (nitrogen) elemental analyses were performed in the analytical chemistry laboratory of Hangzhou University in order to calculate the H/C ratio of carbon nanotubes.

Transmission electron microscope (TEM) and high resolution transmission electron microscope (HRTEM) observation.—Carbon nanotubes were characterized with JEOL 100 CX and JEOL2010 microscopes. High-resolution images were recorded with a side-entry JEOL2010 TEM with a point-to-point resolution of 0.19 nm operated at 200 kV. The specimens for TEM were either directly glued onto Cu grids or dispersed in acetone by ultrasound, and then dropped on the carbon grids with holes.

X-ray diffraction measurements.—X-ray diffraction (XRD) measurements were performed with a Philips diffractometer PW1710 with Cu $K\alpha_1$ radiation (1.5418A). L_c was estimated by the Scherrer equation, $L_{hkl} = 0.9\lambda/(\beta \cos \theta)$, where λ is the X-ray wavelength, θ is the Bragg angle, and β is the half-peak width in radians. We used the (002) peak to calculate L_c.

Raman spectra measurements.—The Raman spectra (RS) were excited with 150 Mw of 514.5 nm radiation from an Ar-ion laser, and the scattered light was dispersed with a V1000 ISA double spectrometer. The sample geometry for the RS measurements was a disk with a diameter of 3 mm and a thickness of 0.5 nm prepared by pressing the powder under a nominal pressure of 3.1 GPa. The Lorrentzian function was used exclusively to fit the spectra in this study. The peak integrals were computed either directly from the spectra or derived from the band parameters calculated during the fitting process.

* Electrochemical Society Active Member.

S0013-4651(98)08-024-0 CCC: $7.00 © The Electrochemical Society, Inc.

Electrochemical testing.—All electrochemical measurements were carried out using coin-type test cells. Cells were assembled in an Ar-filled glove box. Carbon nanotubes were used as positive electrodes, and Li foils were used as negative electrodes. The electrolyte was 1 M $LiClO_4$ dissolved in a 50/50 (vol %) mixture of ethylene carbonate and diethyl carbonate. Positive electrodes were prepared by using foam Ni as the support matrix, and using polytetrafluoroethylene (PTFE) as the binder. A slurry of 92 wt % carbon nanotubes and 8 wt % polytetrafluoroethylene (PTFE) diluted in anhydrous alcohol was uniformly spread onto preweighed foam nickel flakes and dried at 100°C for several hours. These stocks were compressed between flat plates to ~30 bar pressure and dried at 150°C under vacuum overnight, and then weighed to determine the active mass of carbon. Cells were tested using computer-controlled constant-current cyclers between 0.005 and 2.800 V at 25°C. During the first three discharge/charge cycles, Li/carbon nanotubes cells were tested at a constant current of 20 mA/g. More rapid cycling of cells, to determine cycle life, was performed at a higher current of 40 mA/g.

Results and Discussion

Morphology and microstructure of carbon nanotube.—A sample designated as "A" was obtained by pyrolysis of acetylene catalyzed by iron nanoparticles. A sample designated as "B" was obtained by pyrolysis of ethylene catalyzed by iron oxide nanoparticles. The TEM images in Fig. 1a and b show that the morphologies of samples A and B are central hollow cylinders with diameters of about a few tens of nanometers. The diameter of sample A is about 30 nm, and that of sample B is about 12 nm. The yield of carbon nanotubes is above 90% (vol %) estimated from random sampling and repeated TEM observations. The HRTEM image in Fig. 2a shows a typical microstucture of sample A, in which the graphitic planes are packed at fixed angles to the central core. Wrinkled graphite sheets (arrow a) can be found in sample A by a tracing of the lattice fringes. The wrinkled layers can be attributed to interstitial carbon atoms between graphitic planes,[15] because the atoms in the graphite plane are attracted to the interstitial carbon atoms, but the nearest neighbors are forced to the opposite direction.[16] An unorganized graphitic structure (arrow b) also exists in sample A where the lattice fringes are disordered. "Unorganized carbon" may consist of bulk single layers or of tetrahedrally bonded carbon.[17] Microcavities (arrow c) could be formed at the edges of the graphitic planes and in the region of unorganized carbon.[18,19] The selected-area electron diffraction pattern in the inset shows that the spacing between the layers (d_{002}) of sample A is 0.352 nm. Sample B consists of about ten concentric shells of graphitic sheets (Fig. 2b), which lie parallel to the central core with 0.344 nm spacing between the sheets, confirmed by the selected-area electron diffraction pattern in the inset. Few defects and disordered structures can be observed in Fig. 2b. The XRD patterns of samples A and B are shown in Fig. 3a and b, respectively. The d_{002} values of sample A and sample B derived from XRD patterns are 3.52 and 3.45 nm, respectively, which are consistent with the values obtained from selected-area electron diffraction patterns. The L_c values of sample A and sample B from XRD are 1.4 and 2.4 nm, respectively. From selected-area electron diffraction patterns, XRD patterns, and HRTEM images, we can conclude that sample B is more graphitized than sample A and that sample A has a larger d_{002} value than that of sample B, which may be caused by the presence of interstitial carbon atoms between the graphitic planes.[15]

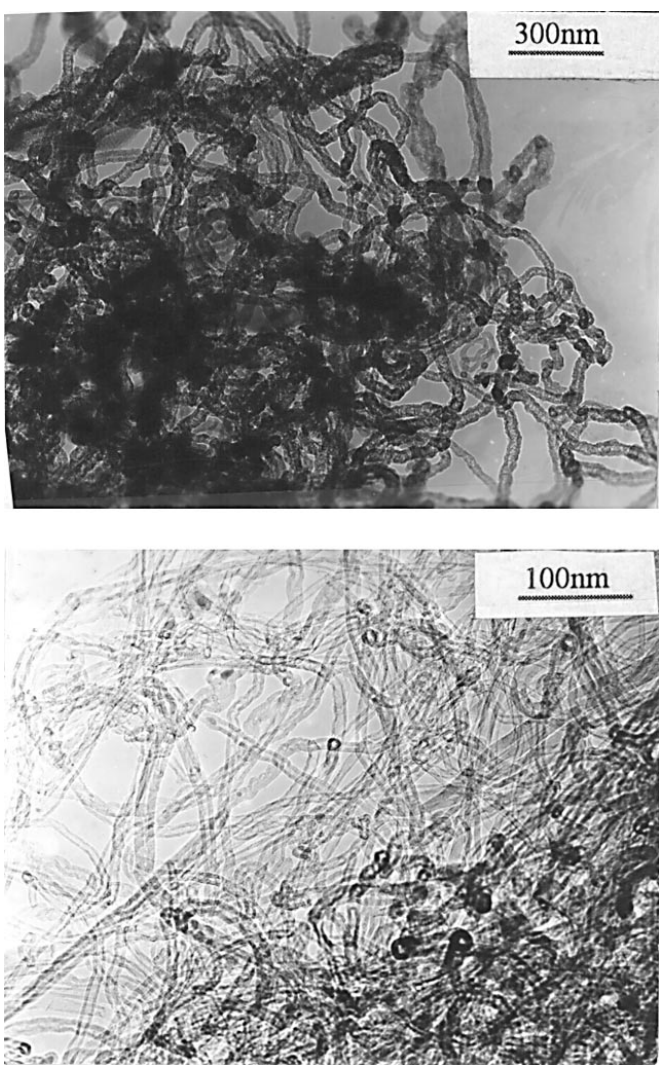

Figure 1. TEM images of carbon nanotubes: (a, top) sample A and (b, bottom) sample B.

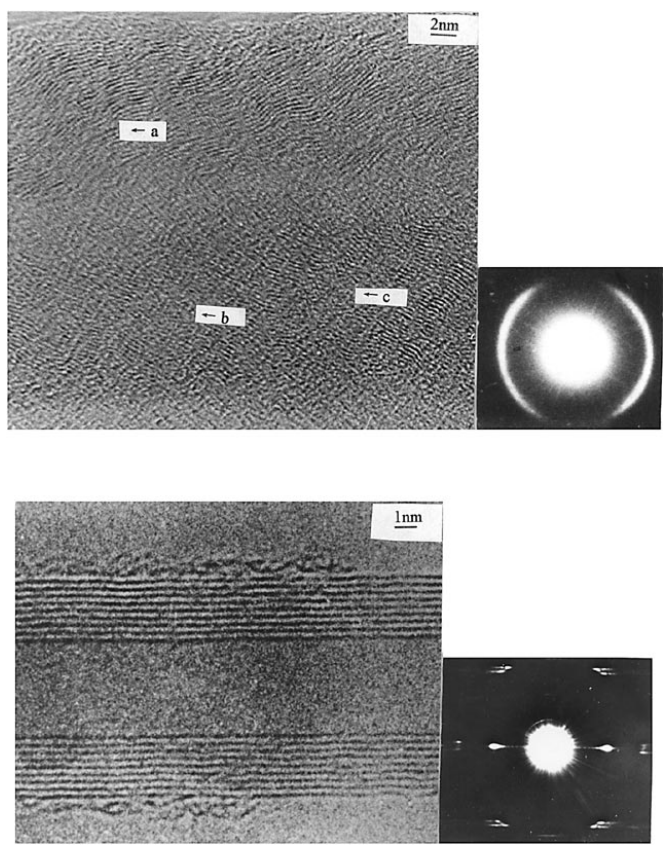

Figure 2. HRTEM images of carbon nanotubes. Right: selected-area electron diffraction pattern; (a, top) sample A and (b, bottom) sample B.

S0013-4651(98)08-024-0 CCC: $7.00 © The Electrochemical Society, Inc.

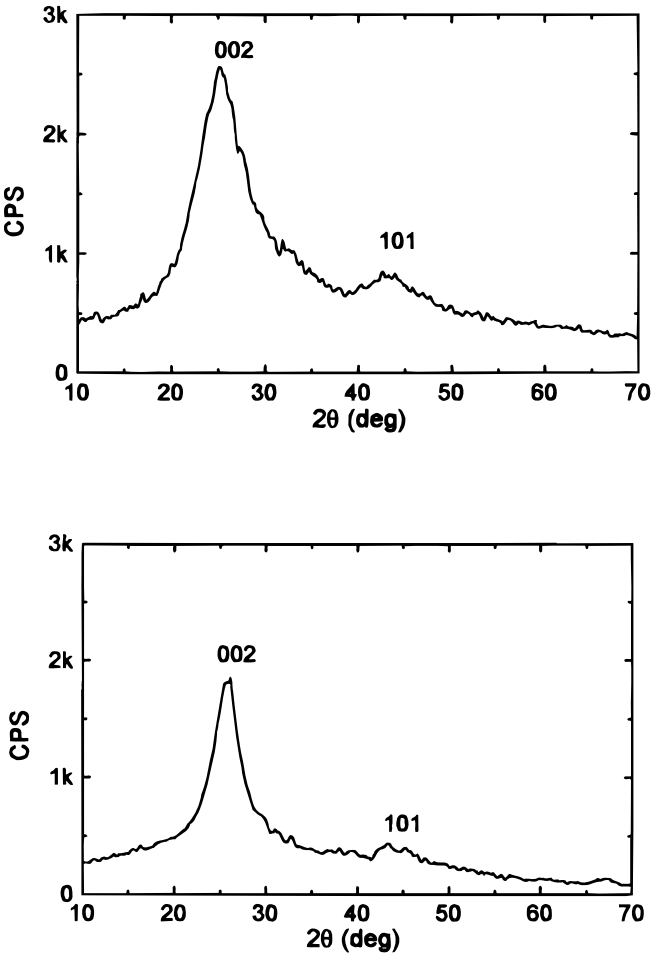

Figure 3. XRD patterns for carbon nanotubes: (a, top) sample A and (b, bottom) sample B.

Raman spectroscopy of carbon nanotube.—Figure 4 shows first-order Raman spectra of the carbon nanotubes. The main Raman lines observed in Fig. 4a and b are at about 1350 and 1580 cm^{-1}. Tuinstra and Koening[8] found that for polycrystalline graphite the intensity ratio of the 1350 cm^{-1} line and the 1580 cm^{-1} line ($R = I_D/I_G$) is inversely proportional to the effective crystallite size in the direction of the graphite plane (L_a) and L_a was calculated by the empirical formula $L_a = 4.4/R$. Although this empirical formula was not suitable for analyzing carbon nanotubes[9] due to the curved nature of graphite layers in carbon nanotubes, we believe that the value of R can be used to estimate the extents of graphitization of the carbon nanotubes. In the present case, the values of R from the Raman spectra of carbon nanotubes are 1.2 for sample A and 0.7 for sample B, which reflects that sample B is more graphitized than sample A.

In Fig. 4, the Raman line near 1580 cm^{-1} of sample A is broad and upshifted in frequency compared with that of sample B. The pronounced linewidth broadening and frequency upshift of sample A is associated with an additional Raman line at 1620 cm^{-1}. The 1620 cm^{-1} line itself has engendered considerable debate in the literature.[20-22] Nemanich et al.[20] attributed the 1620 cm^{-1} lines to modes corresponding to a high vibrational density of states in graphite. Nakamizo and Tamai believed[21] that the 1620 cm^{-1} band arose from hexagonal ring stretching in very small graphite crystallites with all of their surfaces covered with carbon-oxygen complexes. The 1620 cm^{-1} mode is prominent for graphitic planes bounded by intercalant layers and is the only band observed for stage-1 intercalation compounds where graphite layers are never adjacent to each other.[22] We believe that interstitial carbon atoms are present between the graphitic planes as confirmed by selected-area electron diffraction patterns, XRD patterns, and HRTEM images. Vibration of the graphitic planes bounded by interstitial carbon atoms may lead to the 1620 cm^{-1}.[23,24]

Charge and discharge of carbon nanotube electrode.—Figure 5 shows the first discharge and subsequent charge/discharges of the carbon nanotubes. The first discharge curves of sample A and sample B both show a plateau at about 0.8 V, which may be associated with electrolyte decomposition and causes the formation of a passive film or solid electrolyte interphase (SEI) on the carbon surface.[25] Because the equivalent specific surface areas of sample A and B are very large, about 900 and 875 mAh/g are passed for sample A and sample B to form SEI films on the surfaces during the first discharge, respectively. In subsequent cycles, Li can insert reversibly into the carbon nanotubes. The first charge capacity is 640 mAh/g for sample A and 282 mAh/g for sample B. An amount of Li significantly higher than LiC_6 (372 mAh/g) is electrochemically inserted into sample A. The voltage profiles (Fig. 5) of both sample A and sample B show a large hysteresis, i.e., the lithium was inserted below 0.25 V and removed above 1 V. In order to better reveal features of the potential plateau, dQ/dV (differential capacity) vs. voltage curves are plotted in Fig. 6. A plateau in the voltage profile appears as a peak in the differential curve. The peak corresponding to the 1 V plateau during charge is apparent for sample A, but not apparent for sample B. Dahn et al.[12] reported that Li atoms can bind in the near vicinity of H atoms in hydrogen-containing carbons, which is related to their high capacity and the hysteresis. In the present case, the H/C ratio of sample A and sample B are 0.08 and 0.02, respectively.

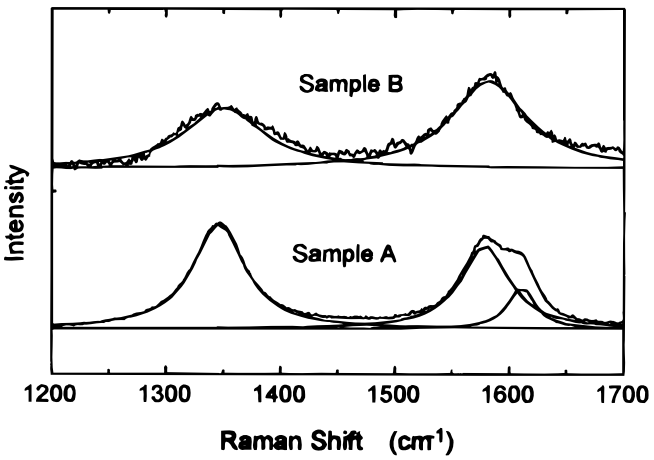

Figure 4. Raman spectra of carbon nanotubes.

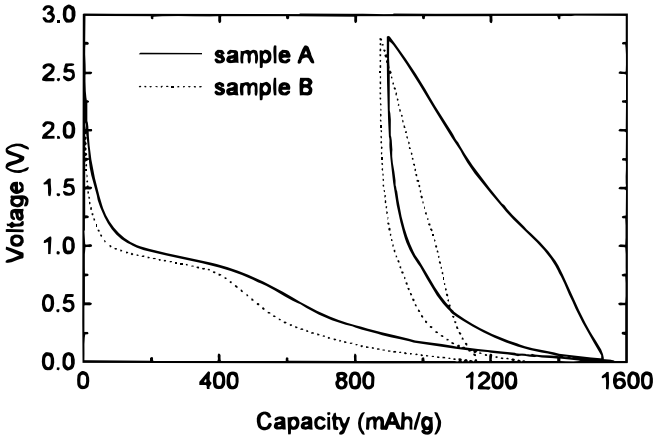

Figure 5. The first discharge and subsequent charge/discharges of carbon nanotubes at 20 mA/g at 25°C.

S0013-4651(98)08-024-0 CCC: $7.00 © The Electrochemical Society, Inc.

The charge capacities of our samples increase as the H/C ratio increases, which agrees with what Zheng et al.[26,27] reported. However, the H/C ratio of sample A is much smaller than that of hydrogen-containing carbons,[26,27] which cannot lead to the specific capacity of 640 mAh/g. According to the arguements in the work reported by Zheng et al.,[26,27] sample A has excess capacity of 180 mAh/g and sample B has excess capacity of 45 mAh/g due to each H atom bonding to a Li atom. However, the charge capacity of sample A is about 258 mAh/g more than that of sample B. So we believe that the high capacity and hysteresis of sample A cannot be simply attributed to the hydrogen in these samples. The higher charge capacity of sample A may be also related to Li being doped mainly into regions without organized graphitic structures,[28] microcavities,[18,19] edges of graphitic layers,[29,30] and surfaces of single graphitic layers.[12] The hysteresis during lithium insertion into sample A may also be related to the interstitial carbon atoms as mentioned in our previous paper.[23,24] The Raman spectra, XRD, HRTEM, and selected-area electron diffraction patterns of sample A showed that there exist interstitial carbon atoms between the graphitic planes of sample A. The interstitial carbon atoms bond to the carbon atoms in aromatic planes. When inserted Li diffuses to the vicinity of interstitial carbon atoms, Li may transfer part of its 2s electron to a nearby interstitial carbon atom, which results in a change of the bond between the interstitial carbon atoms and carbon atoms in the aromatic planes. This would also cause a change in the relative atomic position of interstitial carbon and carbon atoms in aromatic planes. These bonding changes are activated processes, which can lead to hysteresis.[23,24] The hysteresis in the ballmilled sugar carbons was different from that in hydrogen-containing carbons,[30] however Xing et al.[30] did not explain the mechanism of 1 V hysteresis. The 1 V hysteresis in ballmilled sugar carbons may be related to the interstitial carbon atoms as stated in our previous paper.[23,24] They also found that additional capacity between 2 and 3 V may be associated lithium atoms being withdrawn from bonding environments near surface functional groups, such as COOH groups. Our samples have capacities above 2 V, which may be due to the surface functional groups. Because our samples were exposed in air or held in dilute HNO_3 for 4 h, it is very likely that surface functional groups were formed.

Effect of cycling temperature.—Figure 7 shows a comparison of voltage profiles for sample A tested at 40 mA/g and 25, 35, 45, and 55°C. The cell capacity increases with increasing cycling temperature. The extra capacity appears as an increased low-voltage plateau during discharge and an increased 1 V plateau during charge. Corresponding to Fig. 7, *dQ*/*dV* vs. *V* plots are shown in Fig. 8a and b, which shows that peaks corresponding to 1 V plateaus during charge move to lower voltages. However, the peaks corresponding to the low-voltage plateaus during discharge may be below 0.005 V, as shown in Fig. 8b, which renders the peak position unmeasurable. The areas under these two peaks increase with increasing cycling temperature, which confirms that the increases of the low-voltage capacity during discharge and the 1 V capacity during charge lead to the excess capacity with increasing cycling temperature. The peak positions during charge in the differential capacity curve vs. *kT*/*e* are plotted in Fig. 9. As shown in Fig. 9, the position of the peak during charge is inversely proportional to *kT*/*e*, which displays features similar to the hydrogen-containing carbon reported by Zheng et al.[27] We

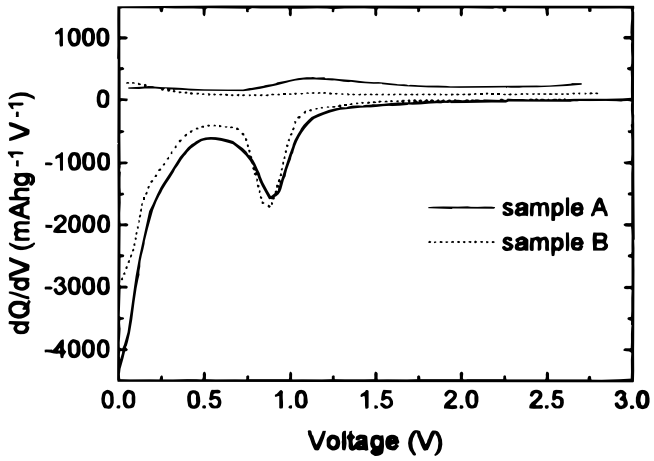

Figure 6. Differential capacity vs. voltage for carbon nanotubes during the first discharge/charge.

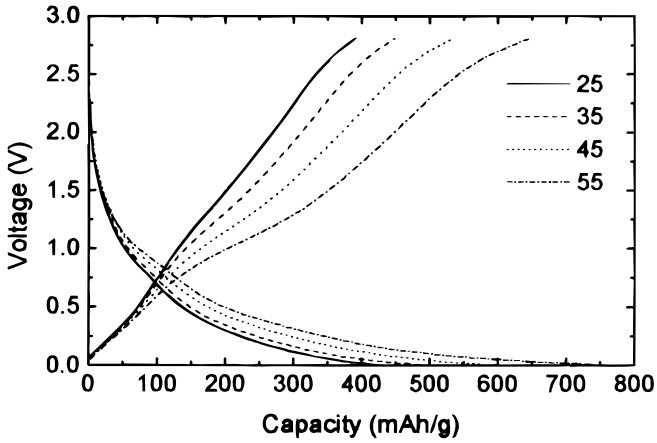

Figure 7. Voltage profiles for sample A tested at different temperatures: 25, 35, 45, and 55°C at 40 mA/g.

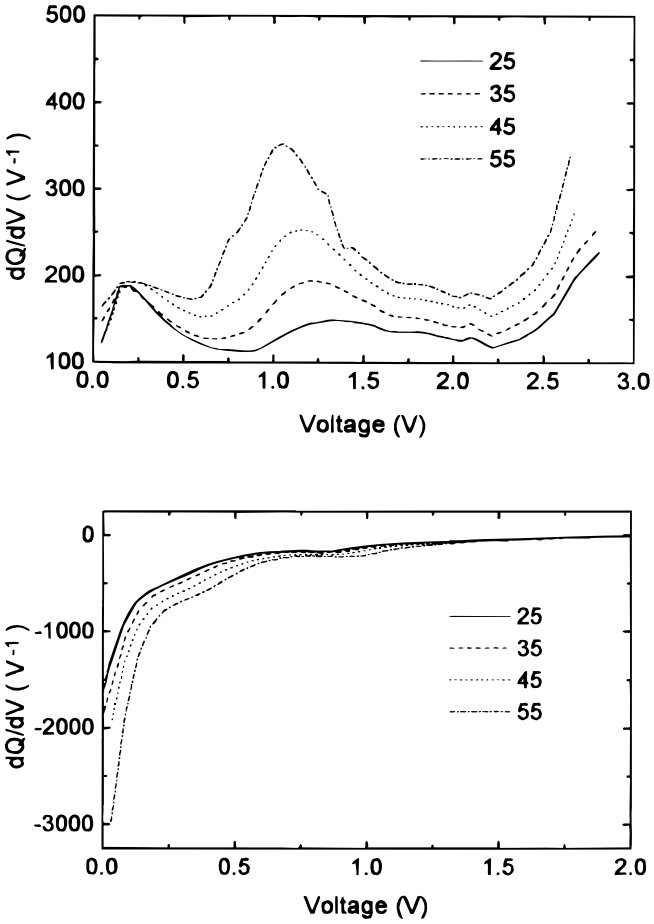

Figure 8. Differential capacity vs. voltage for sample A tested at different temperatures, at 40 mA/g, (a, top) charge and (b, bottom) discharge.

S0013-4651(98)08-024-0 CCC: $7.00 © The Electrochemical Society, Inc.

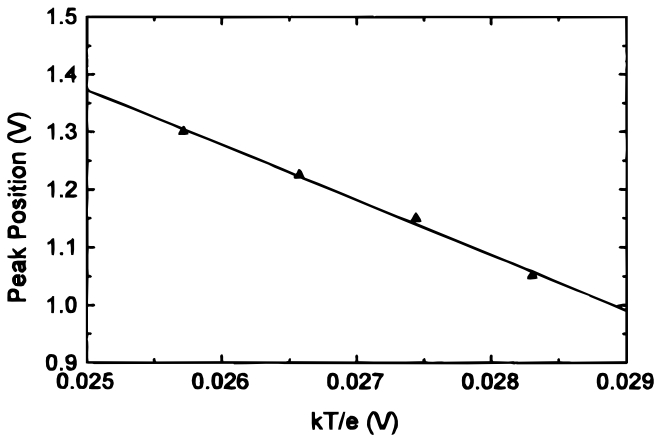

Figure 9. Voltage of the peak in the differential capacity curve vs. *kT*/*e* for the charge of sample A tested at 25, 35, 45, and 55°C.

found that the slope of the line in Fig. 9 (about −95.6 eV) is lower than that of the hydrogen-containing carbon (−62 eV)[27] and that the positions of the peaks in Fig. 8 are higher than those of the hydrogen-containing carbon.[27] The relative positions of these peaks are related to an activated process. The more negative slope and higher positions of these peaks are a result of higher activation energy, which may originate from Li bonding to the interstitial carbon.

Cells made from sample B were also tested at 40 mA/g at 25, 35, 45, and 55°C. The differential capacity vs. the voltage for cells made

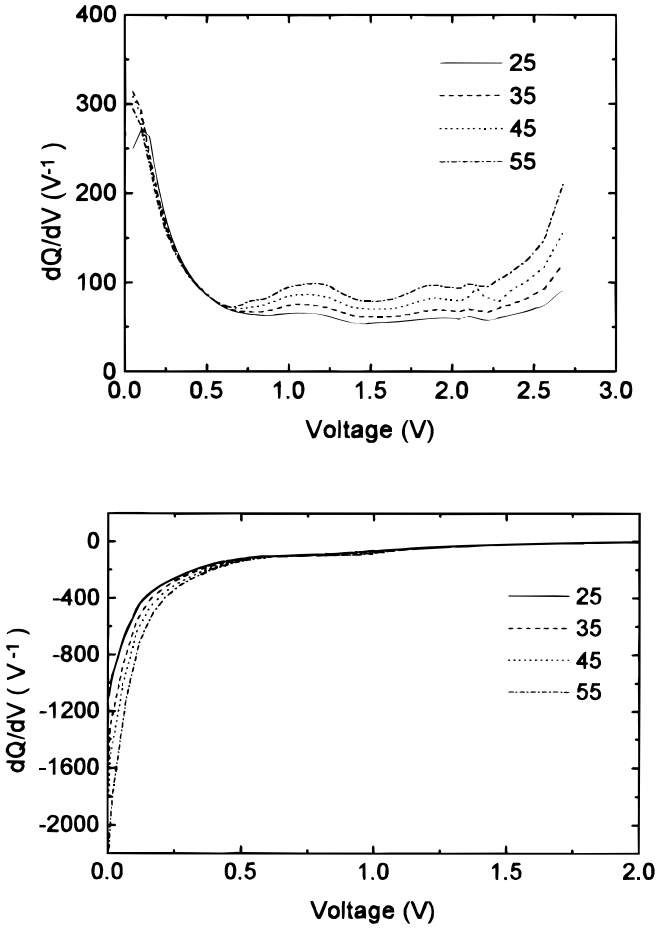

Figure 10. Differential capacity vs. voltage for sample B tested at different temperatures; at 40 mA/g, (a, top) charge and (b, bottom) discharge.

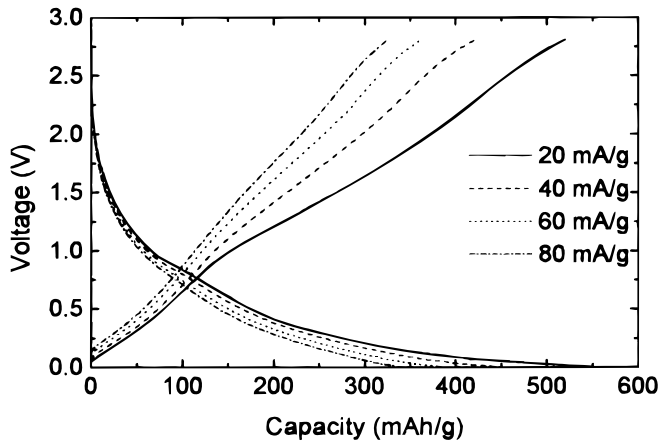

Figure 11. Voltage profiles for sample A tested at different currents at 25°C.

from sample B are plotted in Fig. 10a and b. The peaks corresponding to the 1 V plateaus during charge are invariant with the increasing cycling temperature. The hysteresis of the hydrogen-containing carbon described in Ref. 26 and 27 showed a strong temperature dependence, unlike that observed here.The mechanism for the hysteresis of sample B is not clear, but it may originate from the curved nature of the graphite layers in carbon nanotubes. The charge capacity of sample B increases with the increasing cycling temperature, which may be attributed to overvoltages decreasing with increasing temperature. These overvoltages arise from the ohmic drop in the electrolyte, the liquid-state diffusion of Li in the electrolyte, the solid-state diffusion of Li in the carbon and the impedance associated with the transfer of a Li ion from solution to the electrode. Among these, solid-state diffusion is the dominant factor because the electrical conductivity of carbon nanotubes increases significantly from 25 to 55°C (as the semiconductors), the solid-state diffusion coefficient of Li should increase significantly. The increase of the coefficient leads to decreases of overvoltages and an increase of the charge capacity.

Rate capability of carbon nanotube electrodes.—The voltage profiles for sample A and sample B tested at different currents, 20, 40, 60, and 80 mA/g at 25°C are shown in Fig. 11 and 12, respectively. As the current increases from 20 to 80 mA/g, the cells' capacities decrease sharply. This capacity decrease may be due to increasing overvoltages. A detailed discussion of the various overvoltage is beyond the scope of this paper, and requires more electrochemical measurements. The ratio Q_r/Q_{r20} (Q_r is the charge capacity at a given current, Q_{r20} is the charge capacity at 20 mA/g) vs. cycling currents are plotted in Fig. 13. As shown in Fig. 13, when the cycling current

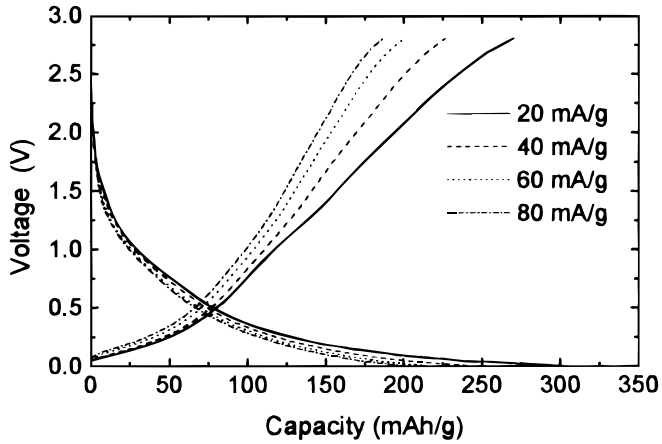

Figure 12. Voltage profiles for sample B tested at different currents; at 25°C.

S0013-4651(98)08-024-0 CCC: $7.00 © The Electrochemical Society, Inc.

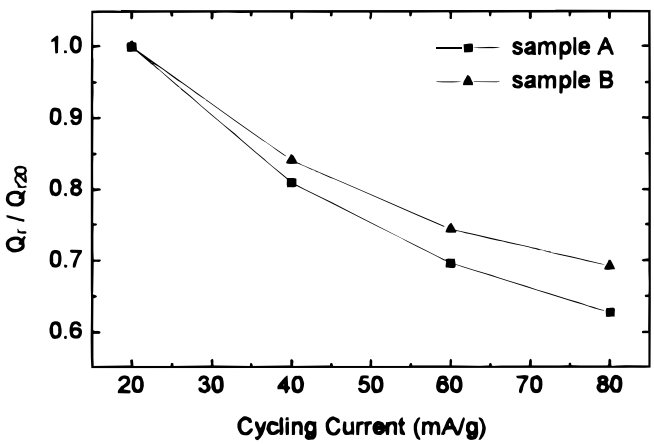

Figure 13. Q_r/Q_{r20} vs. cycling current. (Q_r is the reversible capacity at a certain current. Q_{r20} is the reversible capacity at 20 mA/g.)

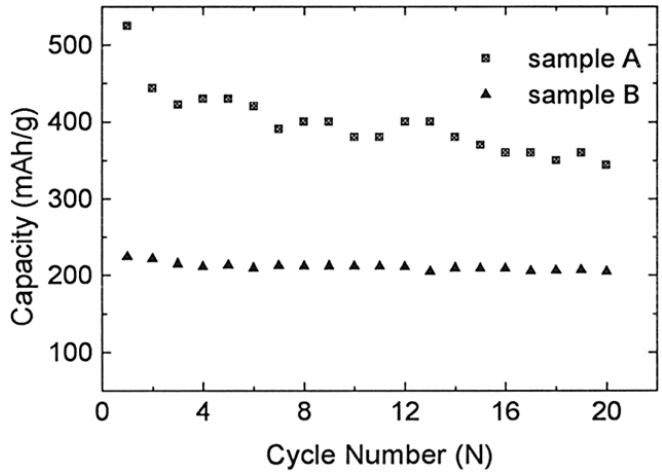

Figure 14. Charge capacity vs. cycle number for cells made from carbon nanotubes at a current of 40 mA/g at 25°C.

increases, the ratio Q_r/Q_{r20} of sample A drops more quickly than that of sample B which shows that the rate capability of sample B is better than that of sample A. The effect of cycling current on the charge capacity near 1 V of sample A leads to poor rate performance of sample A as shown in Fig. 11, which indicates the charge near 1 V of sample A has slow kinetic characteristics.

Cycle life of carbon nanotube electrodes.—Figure 14 shows the charge capacity vs. cycle number of Li/carbon nanotube cells. The cells were cycled at 40 mA/g at 25°C. The charge capacity of sample A degrades quickly during the first three cycles and stabilizes near 400 mAh/g after three cycles. The charge capacity of sample A is only 65.3% of its original value after 20 charge/discharge cycles. However, for sample B the decreases in the charge capacity are very slow. At the end of twentieth cycle, the charge capacity of sample B dropped by only 10%. The difference of cycle life between sample A and sample B may be due to the structure of sample B being more stable than that of sample A.

Conclusions

Carbon nanotubes were produced by pyrolyzing hydrocarbons, such as ethylene and acetylene. The structures of carbon nanotubes were characterized by TEM, HRTEM, XRD, and Raman spectra. Two kinds of carbon nanotubes were found under different reaction conditions. The correlation between structures and Li insertion properties of carbon nanotubes was studied. The charge capacity of the slightly graphitized carbon nanotube is higher than that of the well-graphitized carbon nanotube, but the latter exhibited better cycle life and rate capability. The higher charge capacity of sample A may be related to Li being doped mainly into regions without organized graphitic structures,[28] microcavities,[18,19] edges of graphitic layers,[29,30] and surfaces of single graphitic layers.[12] The slightly graphitized carbon nanotubes showed a 1 V hysteresis, which may be related to Li atoms bonding to the interstitial carbon atoms or H atoms. The positions of the 1 V charge peaks of the slightly graphitized carbon nanotubes in a differential capacity curve were inversely proportional to KT/e. The slope (about -95.6 eV) was lower than that of the hydrogen-containing carbon (-62 eV),[27] and the positions of these peaks are higher than for hydrogen-containing carbon.[27] The more negative slope and higher positions of these peaks were due to the activation energy being higher than that of the hydrogen-containing carbon.

Acknowledgments

The authors acknowledge the financial support from the National Natural Science Foundation of China (grant no. 59502005) and the Natural Science Foundation of Zhejiang university.

Zhejiang University assisted in meeting the publication costs of this article.

References

1. S. Iijima, *Nature*, **354**, 56 (1991).
2. T. W. Ebbesen and P. M. Ajayan, *Nature*, **358**, 220 (1992).
3. M. Endo, K. Takeuchi, S. Igarashi, K. Kobori, M. Shiraishi, and H. W. Kroto, *J. Phys. Chem. Solids*, **54**, 1841 (1993).
4. V. Ivanov, J. B. Nagy, Ph. Lambin, X. B. Zhang, X. F. Zhang, D. Bernaerts, G. Van Tendeloo, S. Amelinckx, and J. Van Landuyt, *Chem. Phys. Lett.*, **223**, 329 (1994).
5. Y. Saito, T. Yoshikawa, S. Bandow, S. Bandow, M. Tomita, and T. Hayashi, *Phys. Rev. B*, **48**, 1907 (1993).
6. D. Reznik, C. H. Olk, D. A. Neumann, and J. R. D. Copley, *Phys. Rev. B*, **52**, 116 (1995)
7. O. Zhou, R. M. Fleming, D. W. Murphy, C. H. Chen, R. C. Haddon, A. P. Ramirez, and S. H. Glarum, *Science*, **263**, 1744 (1994).
8. F. Tuinstra and J. L. Koenig, *J. Chem. Soc.*, **53**, 1126 (1970).
9. J. Kastner, T. Pichler, H. Kuzmany, S. Curran, W. Blau, D. N. Weldon, M. Delamesiere, S. Draper, and, H. Zandbergen, *Chem. Phys. Lett.*, **221**, 53 (1993).
10. H. Hiura, T. W. Ebbesen, and K. Tanigaki, *Chem. Phys. Lett.*, **202**, 509 (1993).
11. P. C. Eklund, J. M. Holden, and R. A. Jishi, *Carbon*, **33**,959 (1995).
12. J. R. Dahn, T. Zheng, Y. Liu, and J. S. Xue, *Science*, **270**, 590 (1995).
13. J. C. Withers, R. O. Loutfy, and T. P. Lowe, *Fullerene Sci. Technol.*, **5**, 1 (1997).
14. V. A. Nalimova, D. E. Skovsky, G. N. Bondarenko, H. Alvergnt-Gaucher, S. Bonnamy, and F. Beguin, *Synth. Met.*, **88**, 89 (1997).
15. J. Lachter and R. H. Bragg, *Phys. Rev. B*, **33**, 8903 (1986).
16. J. Abrahamson and R. G. A. Maclagan, *Carbon*, **22**, 291 (1984).
17. R. E. Franklin, *Proc. R. Soc., London Ser. A*, **209**, 196 (1951).
18. A. Mabuchi, K. Tokumitsu, H. Fujimoto, and T. Kasuh, *J. Electrochem. Soc.*, **142**, 1041 (1995).
19. K. Tokumitsu, A. Mabuchi, H. Fujimoto, and T. Kasuh, *J. Electrochem. Soc.*, **143**, 2235 (1996).
20. R. J. Nemanich and S. A. Solin, *Phys. Rev. B*, **20**, 392 (1979).
21. M. Nakamizo and K. Tamai, *Carbon*, **22**, 197 (1984).
22. M. S. Dresselhaus and G. Dresselhaus, *Adv. Phys.*, **30**, 290 (1981).
23. C. S. Wang, G. T. Wu, X. B. Zhang, Z. P. Qi, and W. Z. Li, *J. Electrochem. Soc.*, **145**, 2751 (1998).
24. C. S.Wang, G. T. Wu, and W. Z. Li, *J. Power Sources*, In press (1998).
25. R. Fong, U. von Sacken, and J. R. Dahn, *J. Electrochem. Soc.*, **137**, 2009 (1990).
26. T. Zheng, Y. Lu, E. W. Fuller, S. Tseng, U. von Sacken, and J. R. Dahn, *J. Electrochem. Soc.*, **142**, 2581 (1995).
27. T. Zheng, W. R. Mckinnon, and J. R. Dahn, *J. Electrochem. Soc.*, **143**, 2137 (1996).
28. M. Inaba, H. Yoshido, and Z. Ogumi, *J. Electrochem. Soc.*, **143**, 2572 (1996).
29. H. Q. Xiang, S. B. Fang, and Y. Y. Jiang, *J. Electrochem. Soc.*, **144**, L187 (1997).
30. W. Xing, R. A. Dunlap, and J. R. Dahn, *J. Electrochem. Soc.*, **145**, 62 (1998).